Effects of Individual and Combined Additions of Pb, Bi, and Sn on the Microstructure and Mechanical Properties of Al-10.8Si-2.25Cu-0.3Mg Alloy

A.M.A. MOHAMED, F.H. SAMUEL, A.M. SAMUEL, and H.W. DOTY

The effects of individual and combined additions of Pb, Bi, and Sn on the microstructure and mechanical properties of the modified grain-refined Al-10.8 pct Si alloy were investigated. Microstructures were monitored using optical microscopy and electron probe microanalysis (EPMA) techniques. Mechanical properties of as-cast and heat-treated alloys were evaluated using hardness measurements and tensile testing. The results show that Pb alone has no significant effect on the microstructure and mechanical properties in the as-cast and heat-treated conditions; Bi counteracts the modifying effect of Sr, leading to coarsening of the eutectic Si particles; however, Sn precipitates as β-Sn within the Al_2Cu network when added individually. Lead and bismuth combined precipitate as bismuth particles enveloped with Pb_3Bi phase, thereby improving mechanical properties in the as-cast and aged conditions contrary to the combined addition of Bi and Sn. Tin and indium combined precipitate as In_3Sn phase, thereby providing better mechanical properties in as-cast and aged conditions than may be obtained through the addition of Sn alone.

DOI: 10.1007/s11661-008-9692-1

I. INTRODUCTION

ALUMINUM alloys are widely used in the automotive industry nowadays, since recent trends incline toward achieving higher performance without increasing weight. Thus, automotive components are increasingly being made of aluminum alloys in order to reduce overall weight, while at the same time maintaining or improving mechanical properties. Apart from their excellent casting characteristics, as well as their wear and corrosion resistance, aluminum-silicon (Al-Si) casting alloys are used so extensively because they also impart a wide range of mechanical properties and high strength to weight ratio.[1–3] Near-eutectic Al-Si casting alloys have increasingly attracted attention because of their excellent castability and lower cost compared with A356 alloys.[3–5]

The production of near-eutectic Al-Si alloys with improved quality (better structure and mechanical properties) involves the application of two major processes: (1) addition of alloying elements during the melting stage and melt treatment (grain refining and modification) or (2) heat treatment.[4,5] The addition of certain elements, such as calcium (Ca), antimony (Sb), sodium (Na), and strontium (Sr), to near-eutectic Al-Si alloys has the effect of altering or *modifying* the morphology of eutectic silicon from an acicular platelike form to a fibrous form. This change in Si morphology enhances the mechanical properties of the alloy, in particular, its ductility.[6] In recent years, the use of Sr as a modifier, instead of Na and Sb, has become a widely accepted practice, although Sr has been reported to have an incubation-time problem.[5,7,8] However, it is worth noting that at the same time as eutectic silicon particles change from acicular to fibrous, the amount, morphology, and size of the dendritic α-Al phase are also affected. It was thought in error that it was enough to only modify the eutectic Si phase in near-eutectic Al-Si alloys, and not necessary to refine the dendritic α-Al phase; but in fact, at the same time that the morphology and size of the eutectic silicon phase is transformed by the modification treatment, considerable changes to the amount, shape, and size of the α-Al phase also occur.[9] Previous investigations suggest that the addition of Sr to hypoeutectic and near-eutectic Al-Si alloys may promote the columnar growth of the dendrites, which are present in the form of fine slender highly-branched columnar grains; addition of Sr may also result in a noticeable increase in the amount of the dendritic α-Al phase.[2,6] Thus, with regard to such alloys dendrite refinement is a necessary step. The master alloy Al-5Ti-1B, which is an effective grain refiner for pure aluminum and wrought aluminum alloys, is often used in Al-Si cast alloys to obtain fine equiaxed grains. Particles of TiB_2 or $TiAl_3$ from the Al-5Ti-1B master alloy are thought to be capable of acting as the nuclei for α-Al.[10–12] No final conclusion has yet been reached, however, on whether the transition of dendritic α-Al from a long columnar morphology to a fine equiaxed one results in improved mechanical properties in near-eutectic Al-Si alloys.[5]

A.M.A. MOHAMED, Doctor, and F.H. SAMUEL and A.M. SAMUEL, Professors, are with Département des sciences appliqués, Université du Québec a Chicoutimi, 555, boulevard de l'Université, Chicoutimi, PQ, Canada G7H 2B1. Contact e-mail: madel@uqac.ca H.W. DOTY, Doctor, is with GM Powertrain Group, Metal Casting Technology, Inc., Milford, NH 03055.

Manuscript submitted May 2, 2008.
Article published online November 12, 2008

Free-cutting aluminum alloys are used for machining processes.[13–15] These alloys were developed from standard heat-treatable alloys, to which elements for forming additional phases in aluminum matrix were added. These phases (in continuation free machining inclusions) improve the machinability of the material because of the resulting smooth surfaces, lower cutting forces, limited tool wear, and more easily breakable chips. Free machining inclusions are formed through the addition of low melting-point elements to the alloy; these include Pb, Bi, Sn, In, and a number of other elements which are unusable from the practical point of view.[15–17]

The purpose of this research is to examine the modified grain-refined Al-10.8 pct Si near-eutectic alloy as a basis for understanding the role of Pb, Bi, and Sn in more complex systems, which may be employed for industrial applications. In particular, it was shown that it is possible to replace toxic lead by nontoxic tin in an Al-Cu-Bi-Pb alloy, which is one of the most common machinable Al-based alloys.[18] Nevertheless, contrary to Pb, the decomposition sequence of Al-Cu is substantially influenced by the presence of even a small amount of Sn.[19] Solid lubricants, such as graphite and Pb, are dispersed in Al-Si alloys so as to increase their resistance to seizure. However, with the addition of graphite the ductility, formability, and thermal conductivity all tend to decrease.[20] The addition of Sn to Al-Si alloys is capable of meeting many of the described requirements as well as acting as a solid lubricant to minimize the chances of seizure. Murali *et al.*[21] investigated the effect of trace additions of tin, indium, and cadmium on the natural aging of Al-7 pct Si-Mg precipitation-hardened alloy. Delays of up to 24 hours in aging were observed to reduce the final ultimate tensile strength (UTS) by 20 MPa, the yield strength (YS) by 10 MPa, and hardness by 10 to 15 BHN, although elongation was improved by 50 pct. In Al-Si-Cu-Mg alloys, Sn prevented the formation of Mg_2Si, while Sn and Pb prevented the formation of the $Al_xMg_5Cu_4Si_4$ phase. Grebenkin *et al.*[22] also determined that tin is analogous to silicon electronically and replaces silicon in the magnesium compounds Mg_2Si and $Al_xMg_5Cu_4Si_4$.

Mohamed *et al.*[23] investigated the effect of trace additions of Sn on the mechanical properties of B319.2 and A356.2 alloys. Their results show that the higher ductility of Sn-containing alloys in the as-cast condition may be attributed to the stress-strain state of the matrix material associated with fine Sn-bearing phases. The results also show that the mechanical properties of heat-treated B319.2 and A356.2 alloys decrease with increasing Sn content.

There has been limited research on the effect of bismuth on the Al-Si foundry alloys. It was demonstrated that bismuth could serve as an effective eutectic modifier in amounts of 0.2 to 0.25 wt pct Bi in a eutectic Al-Si alloy.[24] It was found, however, that this is not always necessarily the case. Small amounts of Bi (as little as 50 ppm) may interfere with the modification effect of Sr in Al-Si alloy.[25] According to their investigation, it was found that the modification effect (with 100 and 150 ppm Sr) decreases as the amount of Bi additions increases. By 1000 ppm Bi addition, the Sr modification effect was completely eliminated.

To the date of this writing, limited information has been available regarding the effect of the described elements on the mechanical properties of alloys and how these affect manufacturing characteristics such as alloy machinability.[26] Hence, this information cannot be used as a means to control the properties and improve the manufacturing conditions of alloys. It is, therefore, of distinct utility to carry out an evaluation on the effects of the Al-insoluble elements Pb, Bi, Sn, and In (all of which have extremely low distribution coefficients in both Al and Si) on the microstructure and mechanical properties of an experimental Al-10.8 pct near-eutectic alloy to fill part of the gap existing in this knowledge. A thorough understanding of the role of these elements in the alloys studied would make it possible to select material and workpiece designs to obtain optimum machining combinations critical to maximum productivity.

II. EXPERIMENTAL PROCEDURES

The as-received Al-10.8 pct Si ingots were cut into smaller pieces, cleaned, dried, and melted in charges of 34 kg each to prepare the required alloys. The melting process was carried out in a SiC crucible of 40-kg capacity, using an electrical resistance furnace. The melting temperature was maintained at 750 ± 5 °C. All alloys were grain-refined by adding 0.20 pct Ti as Al-5 pct Ti-1 pct B in rod form and modified by adding 150 ppm Sr in the form of an Al-10 pct Sr master alloy using a perforated graphite bell. Taking the grain-refined and modified alloy (coded RGM) as a reference, additions of Pb, Bi, Sn, and In were then made to the RGM alloy in order to study the effects of these elements on the microstructure and mechanical properties of the grain-refined and modified alloy. These elements were added in the form of pure metals, in amounts calculated to obtain the desired compositions. Table I lists the chemical analyses of the various alloys studied and their respective codes, as obtained from samplings for chemical analysis taken from the corresponding melts.

The degassed melt was carefully poured into (a) two preheated (450 °C) L-shaped rectangular graphite-coated metallic molds, for preparing castings/samples for metallographic and hardness measurements, and (b) an ASTM B-108 permanent mold to obtain castings for tensile testing. For each pouring/casting, a sampling for chemical analysis was also taken simultaneously to obtain the corresponding alloy melt composition. The chemical analysis was carried out using arc spark spectroscopy at the GM facilities (Milford, NH).

From each of the castings prepared for metallographic observations, two samples measuring 25 × 25 mm were sectioned off to represent each alloy condition. One sample was used in the as-cast condition, while the second sample was solution heat treated at 495 °C for 8 hours and then immediately quenched in warm water (~65 °C). Microstructures of the polished sample surfaces were examined using an Olympus PMG3 optical microscope (Olympus PMG3, Olympus,

Table I. Chemical Composition of the Various Al-10.8 pct Si Alloys Prepared for This Research

Alloy Code	Chemical Composition (Wt Pct)											
	Si	Cu	Mg	Fe	Mn	Sr	Ti	Sn	Bi	Pb	In	Al
RGM	10.92	2.138	0.373	0.429	0.471	0.030	0.22	0.0	0.0	0.0	0.0	bal
RP	10.82	2.33	0.32	0.4	0.51	0.028	0.27	0.0	0.0	0.43	0.0	bal
RB	10.89	2.21	0.34	0.38	0.49	0.027	0.25	0.0	0.57	0.0	0.0	bal
RN	10.71	2.37	0.32	0.43	0.48	0.031	0.25	>0.48	0.0	0.0	0.0	bal
RPB	10.85	2.35	0.33	0.41	0.50	0.028	0.25	0.0	0.55	0.46	0.0	bal
RBN	10.90	2.24	0.38	0.46	0.49	0.024	0.25	>0.48	0.57	0.0	0.0	bal
R2BN	10.62	2.21	0.33	0.42	0.49	0.023	0.26	>0.48	0.53	0.0	0.0	bal
RNN	10.91	2.20	0.33	0.41	0.51	0.028	0.25	>0.48	0.0	0.0	0.50	bal

Carson, MO). The eutectic silicon particle characteristics including area, length, aspect ratio, roundness, and density were measured and quantified using a LECO*

*LECO is trademark of Leco Corporation, St. Joseph, MI.

2001 image analyzer system in conjunction with the optical microscope. For each sample, 50 fields at a magnification of 500 times were examined so as to cover the entire sample surface in a regular and systematic manner.

Phase identification was carried out using electron probe microanalysis (EPMA) in conjunction with wavelength dispersive spectroscopic (WDS) analyses, using a JEOL** JXA-8900l WD/ED combined micro-

**JEOL is a trademark of Japan Electron Optics Ltd., Tokyo.

analyzer operating at 20 kV and 30 nA, where the electron beam size was ~2 μm. Mapping of certain specific areas of the polished sample surfaces was also carried out where required to show the distribution of different elements in the phases.

Thirty-five bars were prepared for each alloy composition. The test bars were divided into seven sets: one set was kept in the as-cast condition, while the other six sets were solution heat treated at 495 °C for 8 hours, then quenched in warm water at 65 °C, followed by artificial aging at 155 °C, 180 °C, 200 °C, 220 °C, and 240 °C for 5 hours (*i.e.*, T6 and T7 tempered). The solution and aging heat treatments were carried out in a forced-air Blue M Electric Furnace equipped with a programmable temperature controller (±2 °C). The aging delay was less than 10 seconds. For each individual heat treatment, five test bars were used. These procedures were followed for the heat treatment of the hardness and tensile test samples.

Hardness test bars measuring 2.54 × 2.54 × 7.62 cm were cut from the casting. The hardness measurements were carried out on the as-cast and heat-treated samples using a Brinell hardness tester (Brinell Co., Brinell, PA), employing a steel ball of 10-mm diameter and a load of 500 kgf applied for 30 seconds. An average of eight readings obtained from two perpendicular surfaces was taken to represent the hardness value in each case.

The as-cast and heat-treated test bars were pulled to fracture at room temperature at a strain rate of 4×10^{-4}/s using a Servohydraulic MTS Mechanical Testing machine (MTS Systems Corporation, Eden Prairie, MN). A strain gage extensometer was attached to the test bar to measure percentage elongation (pct El) as the load was applied. The YS was calculated according to the standard 0.2 pct offset strain, and the fracture elongation was calculated as the pct El over the 50-mm gage length. The UTS was also obtained from the data acquisition system of the MTS machine. The average YS, UTS, or pct El value obtained from the five samples tested was considered as the value representing a specified condition.

III. RESULTS AND DISCUSSION

A. *Characterization of Microstructures*

The as-cast microstructure of modified grain-refined Al-10.8 pct Si alloy is shown in Figure 1(a). Eutectic silicon particles precipitated in the form of fibrous crystals typical of a modified structure constitute the main microstructural feature observed. It can also be observed that iron precipitates in the form of a predendritic α-Fe phase, whereas the copper phase is seen mainly as small pockets of the blocky Al_2Cu phase nucleating either within the aluminum matrix or at the interface of such pre-existing constituents as Si or intermetallic particles. As regards Al_2Cu, the presence of Sr and Mg leads to an increase in the tendency of this phase to segregate in areas away from the eutectic Si regions. The mechanism of Al_2Cu precipitation has been proposed by Samuel *et al.*[27] as follows: during the first stages of solidification, the formation of the α-Al dendritic network is associated with the segregation of Si and Cu in the melt, ahead of the processing dendrite interfaces. When the solidification temperature approaches the eutectic temperature, rounded/fibrous Si particles precipitate, leading to a local concentration of Cu in the remaining areas. They observed that the presence of Sr also leads to segregation of the copper phase in areas free of eutectic Si particles during precipitation, resulting in the slowing of its dissolution during solution heat treatment. Furthermore, due to the segregation, the Al_2Cu phase more often precipitates in the blocky form rather than in the fine eutectic form.[27]

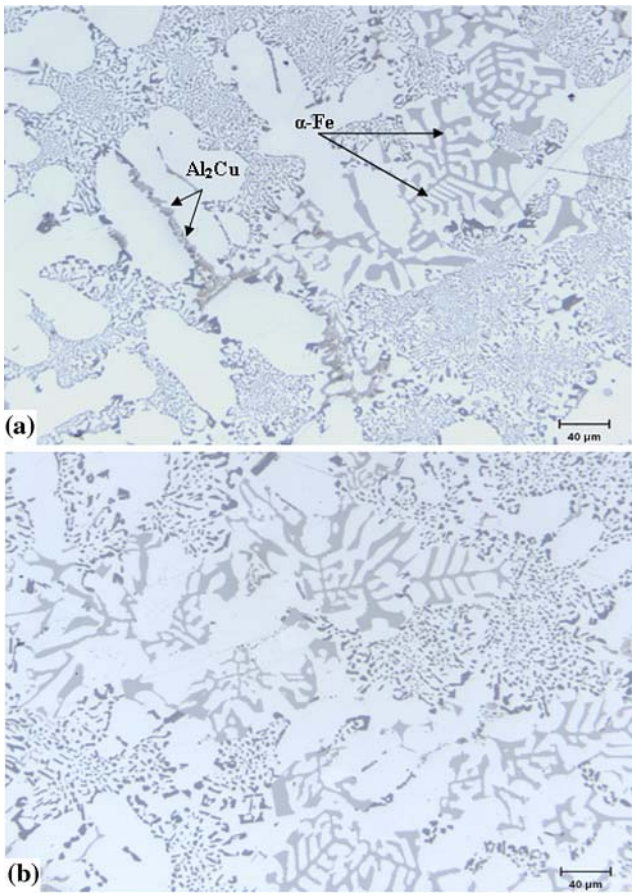

Fig. 1—Typical microstructure of modified grain-refined RGM alloy in (*a*) as-cast and (*b*) solution-heat-treated conditions.

From Figure 1(b), it may be observed clearly that a high degree of spheroidization followed by coarsening occurs during solutionizing at 495 °C. The microstructural changes resulting from solution heat treatment originate from the instability of the interface between two phases. Spheroidization and coarsening of the discontinuous phase occurs at elevated temperatures,[28] because the interfacial energy of a system decreases with the reduction in interfacial surface area per unit volume of the discontinuous phase. The reduction in interfacial energy is the driving force for the spheroidization and the coarsening processes, which are also diffusion-controlled.[29,30] The degree of interconnection of the Si crystals is reduced as spherical and finely dispersed particles are obtained in the aluminum matrix. The changes in size and morphology of the discontinuous silicon phase are significant, since they have a direct influence on the mechanical properties.

1. *Effects on microstructure of adding Pb, Bi, and Sn individually*

Figures 2(a), (c), and (e) show the effects of Pb, Bi, and Sn, respectively, on the microstructure of the modified grain-refined RGM alloy in the as-cast condition. In general, these figures indicate that eutectic Si is somewhat coarse because of the presence of the incompletely modified structures; in particular, Figure 2(c) shows that there is the appearance of acicular needlelike Si formation in RB alloy containing 0.5 pct Bi. Table II summarizes the eutectic Si particle characteristics obtained for the alloys investigated. It may be observed that the addition of 0.5 pct Pb to the RGM alloy (*i.e.*, the RP alloy) leads to a slight coarsening of the eutectic Si particles, as seen in Figure 2(a). For example, the average Si particle area, length, and aspect ratio increase by 17, 14, and 4 pct, respectively, compared to the RGM alloy, whereas the average roundness and density decrease by 4 and 11 pct, respectively.

The addition of 0.5 pct Bi to the RGM alloy counteracts the modifying effect of Sr (Figure 2(c)), leading to a noticeable coarsening of the Si crystals; thus, agreeing with the results obtained by Cho *et al.*[25] The corresponding data on the average particle area showed a jump in this parameter from 2.5 μm^2 in the RGM alloy to 8 μm^2 in the RB alloy. Also, particle length increased from 3 μm in the RGM alloy to 5.5 μm after the addition of Bi. Although no specific bismuth intermetallic compounds were identified in the microstructure of the RB alloy, there is a possibility that a ternary compound, Bi_2Mg_2Sr, or the binary compounds, Bi_3Sr, BiSr, Bi_2Sr_3, and $BiSr_2$ might form, leading to a reduction in the amount of Sr available for modification. Similar observations were reported by Machovec *et al.*,[31] who studied the effect of Bi-Sr interactions on Si morphology for 319-type aluminum alloy.

The addition of 1.1 pct Sn to the RGM alloy is shown in Figure 2(e). A coarser and partially modified eutectic structure is thus to be observed with the addition of 1.1 pct Sn, and the modification level corresponds to that of a class 3 type, namely, partial modification. It may also be observed that there is no significant difference in microstructure between Sn-free and Sn-containing alloys in the as-cast condition except for the precipitation of finely distributed Sn in the form of black reticulate particles of β-Sn (free machining inclusions). These β-Sn particles always solidify within the Al_2Cu network and at the interfaces of Al-α/Si or Al-α/Fe rich intermetallics (Figure 2(e)). The distribution of the β-Sn particles is not uniform; they are distributed in small clusters, thus agreeing with the results obtained by Mohamed et al.[23]

The Al-Sn and Sn-Si alloys both belong to a special binary eutectic system, where there is hardly any solid solubility between Al and Sn or between Sn and Si. With this regard, the Sn content for the eutectic composition of Al-Sn and Sn-Si systems is about 99.8 and 100 pct, respectively, while the corresponding equilibrium temperatures are ~229 °C and ~232 °C, respectively; these temperatures approach, or are equal to, the melting point of Sn.[32] According to the experimental results, there are no Al-Sn compounds to be found in the RN alloy. It may thus be inferred that according to the rules of equilibrium diagrams, the Al-Si-Sn system should belong to a ternary eutectic system. Based on three binary system diagrams and the experimental results, it may be determined that the projection of the ternary eutectic point is near corner Sn. Since the Sn content of the eutectic composition almost approaches 100 pct, the

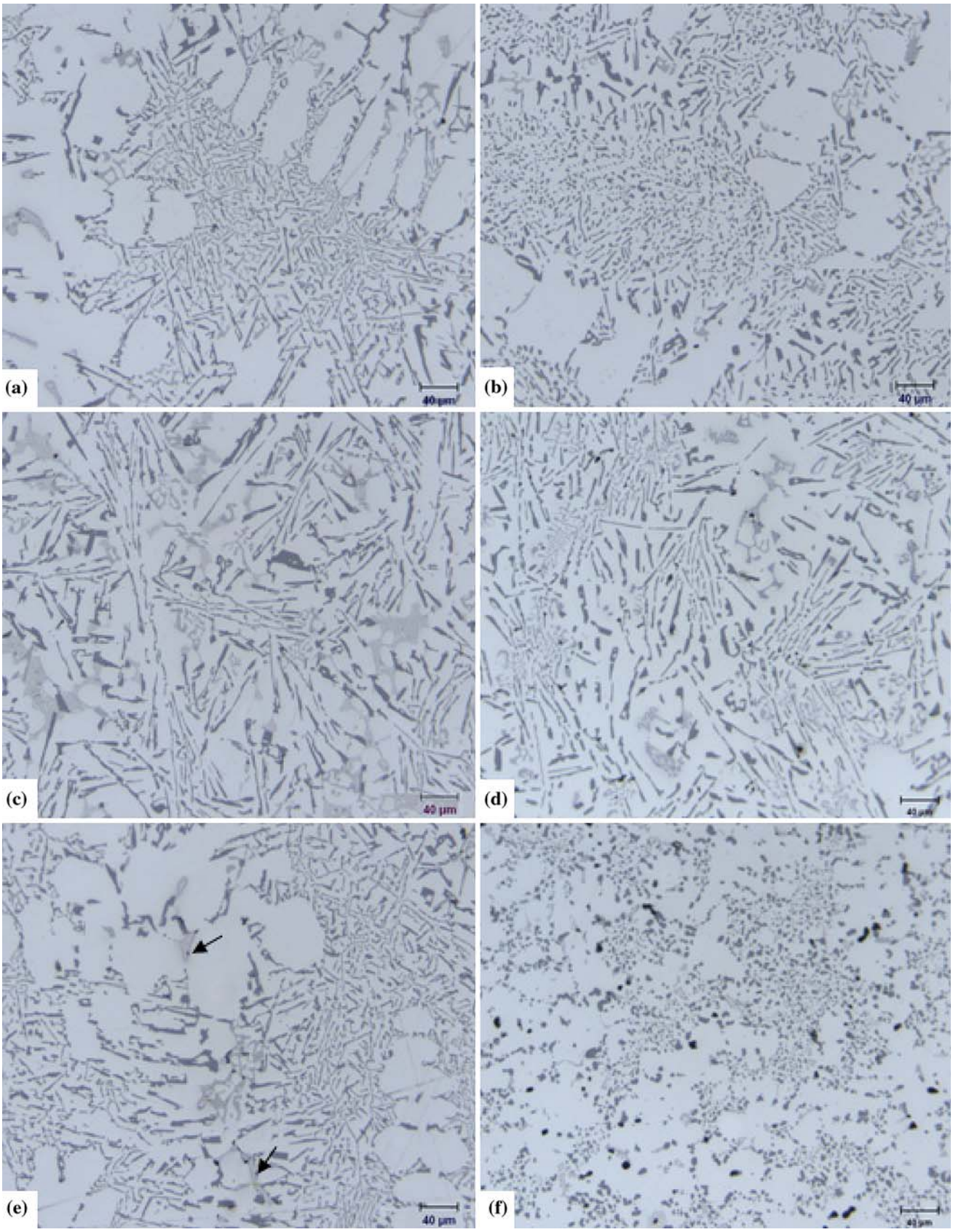

Fig. 2—Typical microstructure of (*a*), (*c*), and (*e*) as-cast and (*b*), (*d*), and (*f*) solution-heat-treated conditions of modified grain-refined RGM alloy with (a) 0.5 pct Pb, (b) 0.5 pct Bi, and (c) 1.1 pct Sn additions.

Table II. Silicon Particle Characteristics of the Alloys

Alloy Code	Solution Time	Particle Area (μm^2)		Particle Length (μm)		Roundness Ratio (Pct)		Aspect Ratio		Density (Particles/ mm^2)
		Av	SD	Av	SD	Av	SD	Av	SD	
R	0*	9	14	7	6	57	29	2.41	1.23	10,096
	8	7	13	6	6	62	20	2.21	1.27	14,457
RGM	0*	2.5	5	3	2.7	71	25	2.11	0.94	40,807
	8	5	7	4	3.3	75	21	1.93	0.84	20,903
RP	0*	3	8	3	4	68	27	2.20	1.04	33,293
	8	6	7	3.5	2.9	73	20	1.96	0.71	20,377
RB	0*	8	14	5.5	6.5	57	32	2.37	1.58	17,855
	8	7	12	5	6	65	19	2.16	0.97	18,965
RN	0*	4	7	3	4.7	67	27	2.28	1.19	25,979
	8	7	6	4	3.7	70	20	2.04	0.83	19,699
RBP	0*	6	11	3	5	61	23	2.28	1.45	23,850
	8	8	10	3.5	4	65	21	2.15	1.41	18,280
RBN	0*	6	12	5	4	59	32	2.34	1.28	20,734
	8	11	14	6	5	64	30	2.12	1.41	15,292
R2BN	0*	5	5	4.5	7	62	33	2.25	1.42	22,116
	8	7	4	5	4	66	29	2.12	1.42	17,672
RNN	0*	4	2	3	2	71	23	2.17	0.83	32,433
	8	6	4	3	2.5	73	20	1.97	0.81	20,226

Note: * = as-cast, Av = average, and SD = standard deviation.

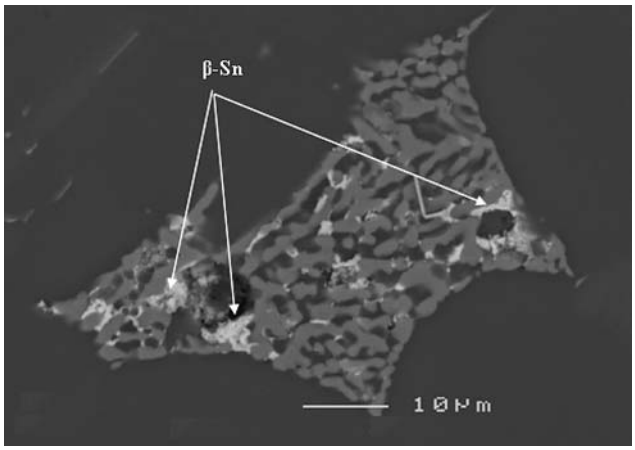

Fig. 3—Backscattered image obtained from RN alloy showing precipitation of β-Sn.

equilibrium temperature should be below 229 °C; it may therefore be concluded that Sn precipitates mainly in the form of the β-phase.

Figure 3 shows a backscattered image of the RN alloy containing 1.1 pct Sn, according to atomic number sequence; the white phases in the matrix are β-Sn, which precipitated within the light gray Al_2Cu network. For further investigation, X-ray mapping of the β-Sn phase was carried out to determine the distribution of Sn, Cu, and Si (Figure 4). The WDS analysis (Table III) suggests that the chemical composition of this phase is β-Sn. Figure 5 shows the backscattered images obtained at high magnification of the RN alloy illustrating the morphology of Sn-containing particles precipitated in the alloy.

It may be seen clearly from Figures 2(b), (d), and (f) that the 8-hour solution heat treatment caused the dissolution of Al_2Cu particles. Upon considering the various stages of the solution treatment as a whole, it can be observed that the three stages of fragmentation, spheroidization, and coarsening may also occur together in the same microstructure, depending upon the variety of Si-particle sizes present in the as-cast structure. Thus, while some longer particles may undergo fragmentation, other smaller Si particles may become spheroidized and those already spheroidized could start coarsening at any particular time during the solution treatment process. As Table II shows, after solution treatment of the RP the average Si particle area and roundness increase, while the aspect ratio and density decrease compared to the as-cast condition (Figure 2(b)). The decrease in Si particle density by 39 pct for the RP alloy may indicate the commencement of the coarsening process. The aspect ratio, defined as the ratio of the length to the width of the particle, decreased with solution heat treatment, thereby leading to shorter more rounded particles.

As may be seen in Figure 2(f), the microstructure of the RN alloy after solution treatment for 8 hours at 495 °C reveals the following: (a) a heightened tendency toward Si-particle spheroidization; (b) the absence of any sign of incipient melting of Cu-base intermetallics; and (c) β-Sn, present in black reticulate form, melts due to solution treatment at 495 °C leading to the formation of spherical voids.

2. *Effects on microstructure of adding Pb, Bi, and Sn in combination*

Table II also summarizes the eutectic Si-particle characteristics obtained from the image analysis

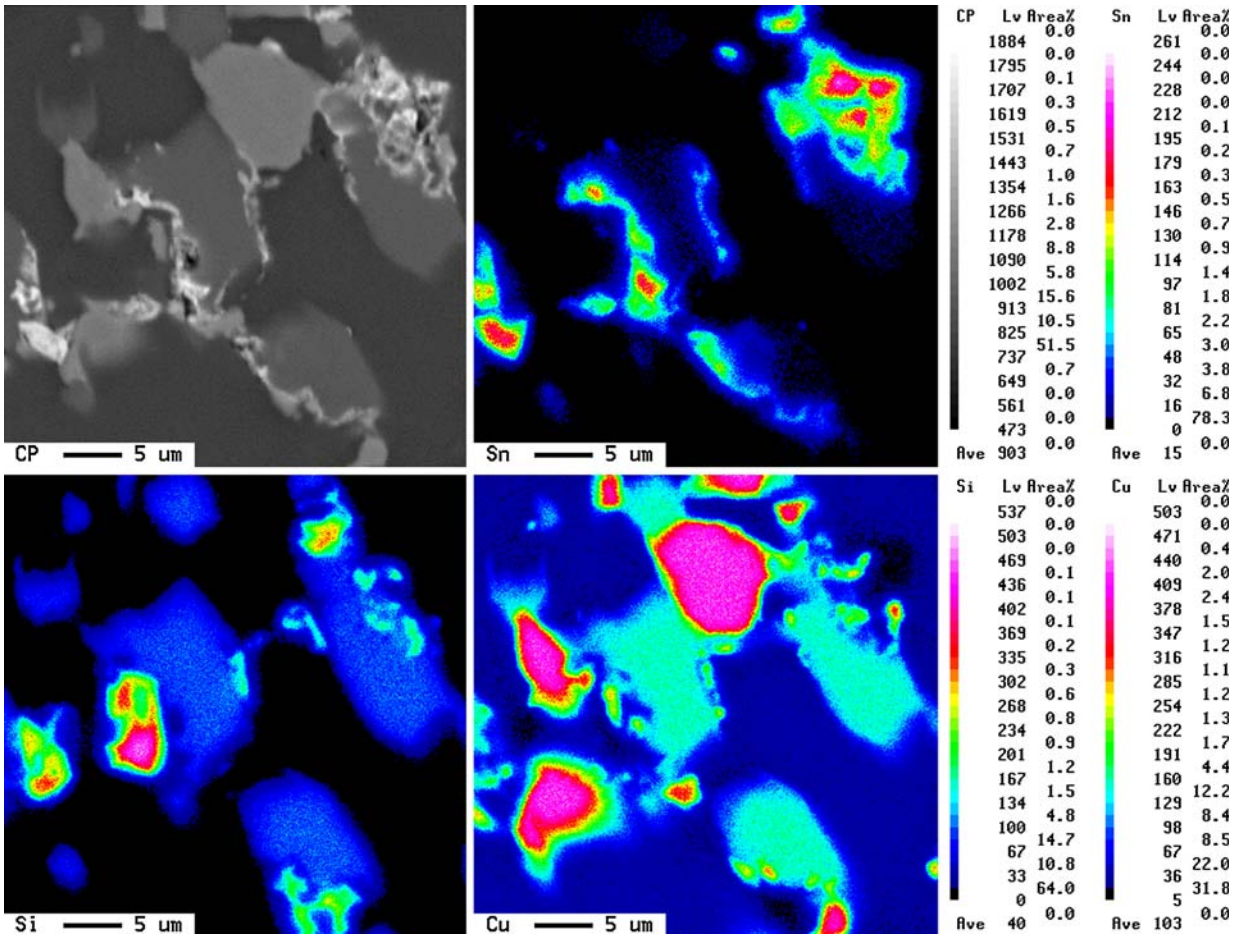

Fig. 4—Backscattered image taken of the RN alloy showing precipitation of β-Sn and the corresponding X-ray image of Sn, Cu, and Si.

Table III. Chemical Composition of the Examined Sn-Containing Phase Particles in As-Cast RN Alloy Obtained from WDS Analysis

Alloy Code	Element	Wt Pct	At. Pct	Color and Shape	Phase
RN	Sn	99 ± 1	96 ± 2	white, reticulate	β-Sn phase
	Cu	1 ± 0.5	2 ± 1		
	total	100	98		

measurements for the RGM alloy with respect to the combined additions of Pb + Bi, Sn + Bi, and Sn + In. It may be observed that such combined additions of elements for the RGM alloy in the as-cast condition have a moderate to significant influence on eutectic Si-particle size, in that the particle size increases in the presence of a combined addition of Pb and Bi (in the RPB alloy) or Sn and Bi (for the RBN alloy), as shown in Figures 6(a) and (b), respectively. A moderate effect may be observed with the combined addition of Sn and In (for the RNN alloy (Figure 6(c)). With respect to the roundness parameter, the best results are obtained with the RNN alloy, which displays the highest roundness values compared to the RBN and RPB alloys.

Figure 7 shows a backscattered image of the RBP alloy (RGM alloy + 0.5 pct Pb + 0.5 pct Bi) in the as-cast condition. Due to a large difference in the atomic numbers (Z), the Pb-Bi particles (free machining inclusions) are easily deciphered as being the brightest with an irregular morphology; they consist of Bi particles enveloped with the Pb_3Bi phase. The high-magnification backscattered image displayed in Figure 8 shows these

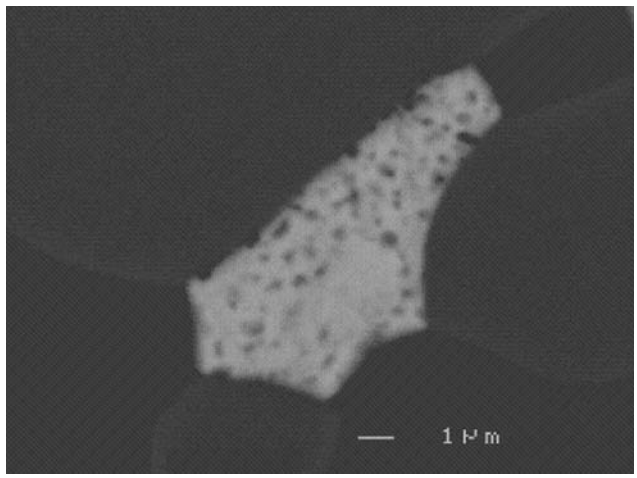

Fig. 5—Backscattered images at high magnification of the RN alloy showing the precipitation of β-Sn.

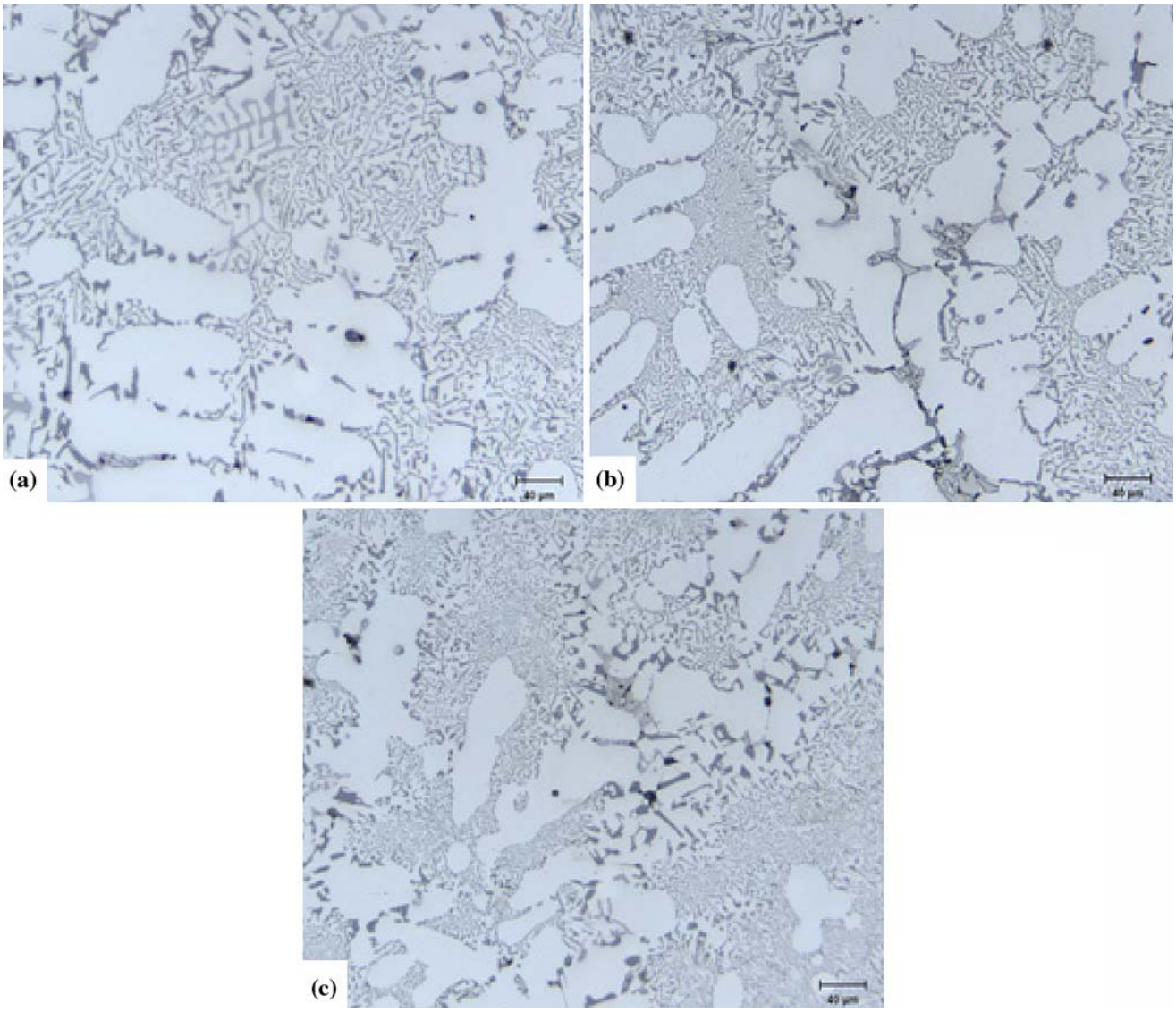

Fig. 6—Typical microstructure of modified grain-refined RGM alloy in as-cast condition with additions of: (*a*) 0.5 pct Pb + 0.5 pct Bi, (*b*) 0.5 pct Bi + 1.1 pct Sn, and (*c*) 0.5 pct Sn + 0.5 pct In.

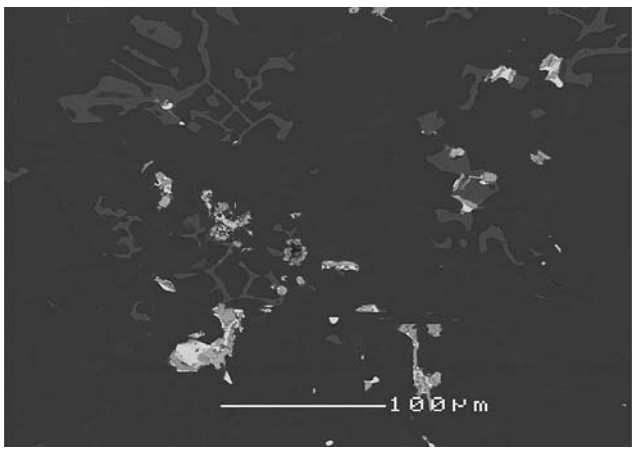

Fig. 7—Backscattered image obtained from RBP alloy showing precipitation of Pb-Bi particles.

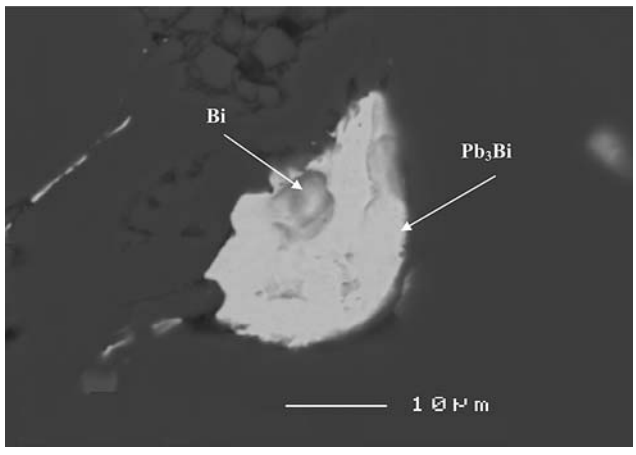

Fig. 8—High-magnification backscattered image taken from RBP alloy (RGM + 0.5 pct Bi and 0.5 pct Pb) showing the presence of a Pb_3Bi particle.

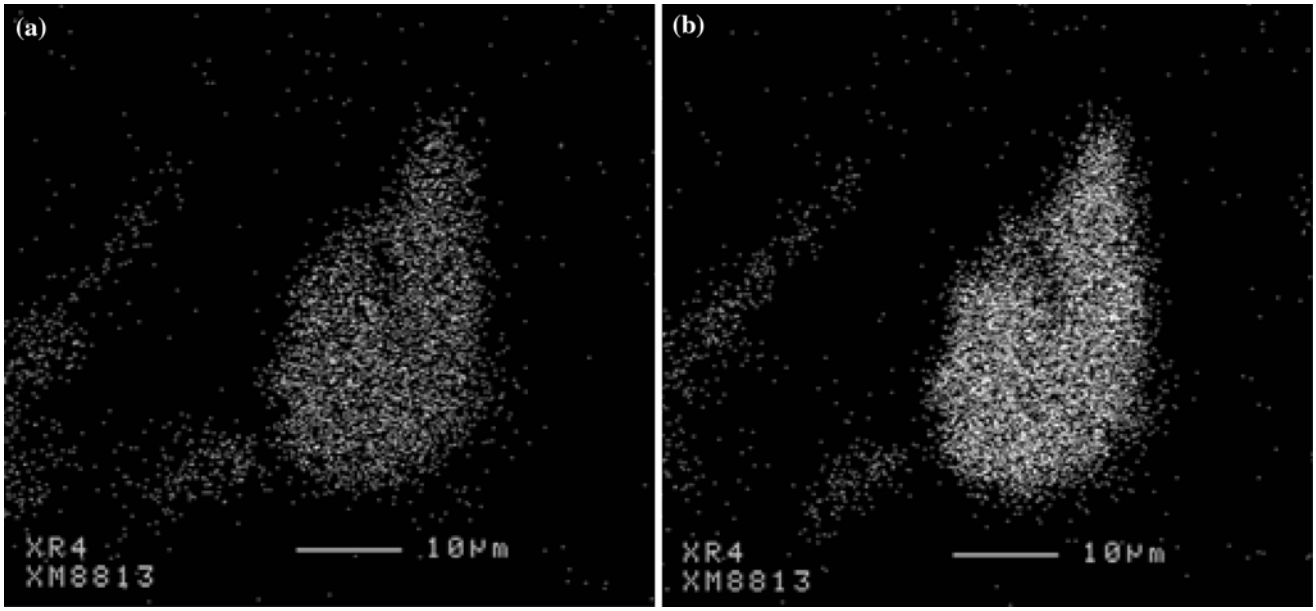

Fig. 9—X-ray images corresponding to the backscattered image showing: (*a*) Bi and (*b*) Pb distribution for the Pb_3Bi particle illustrated in Fig. 8.

Table IV. Chemical Composition of Pb_3Bi Phase Particles in As-Cast RBP Alloy Obtained from WDS Analysis

Alloy Code	Element	Wt Pct	At. Pct	Color and Shape	Phase
RBP	Pb	71 ± 2	73 ± 4.17	bright gray, crescent	Pb_3Bi phase
	Bi	25 ± 3	24 ± 3.9		
	total	96	97		

features clearly. Besides Pb and Bi, these inclusions also contain Al, Cu, and impurity elements. The contents in impurity elements vary from a few tenths to about 1 at. pct. The high Bi and Pb concentrations observed in Figure 9 for the Pb_3Bi particle (Figure 8) are in keeping with the WDS analysis provided in Table IV.

Similar observations may be noted for the In-Sn inclusions observed in the RNN alloy (Figure 10). The backscattered image of the RNN alloy shows a more even distribution of the In-Sn particles, compared to the irregular distribution of the Pb-Bi particles seen in Figure 7. The In-Sn inclusions were smaller and more densely distributed compared to the Pb-Bi inclusions in the RBP alloy. Figure 11 shows a high-magnification backscattered image of the RNN alloy (RGM alloy + 0.5 pct Sn + 0.5 pct In) showing the morphology of the In_3Sn particles, which precipitated in an irregular form. The high In and Sn concentrations observed in Figure 12 for the In_3Sn particles shown in Figure 11 are in keeping with the WDS analysis provided in Table V.

Figure 13 shows the backscattered image corresponding to the optical micrograph seen in Figure 6(b), as taken of the RBN alloy (RGM + 0.5 pct Bi + 1.1 pct Sn). Both figures show the morphology of Bi- and Sn-particles precipitated in the alloy. The distribution of Bi- and Sn-containing particles is shown in Figure 14,

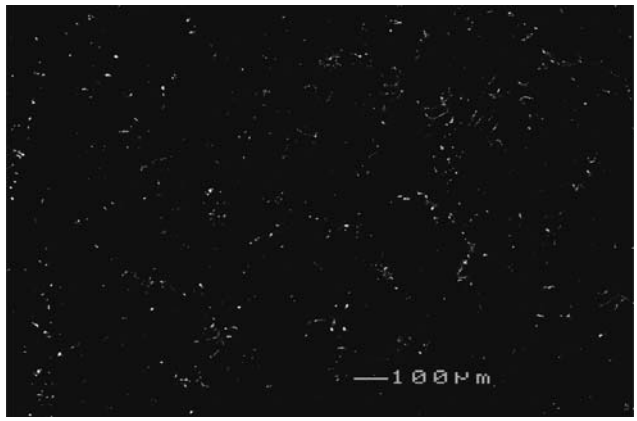

Fig. 10—Backscattered image obtained from RNN alloy containing 0.5 pct Sn + 0.5 pct In showing precipitation of In-Sn particles (bright white spots).

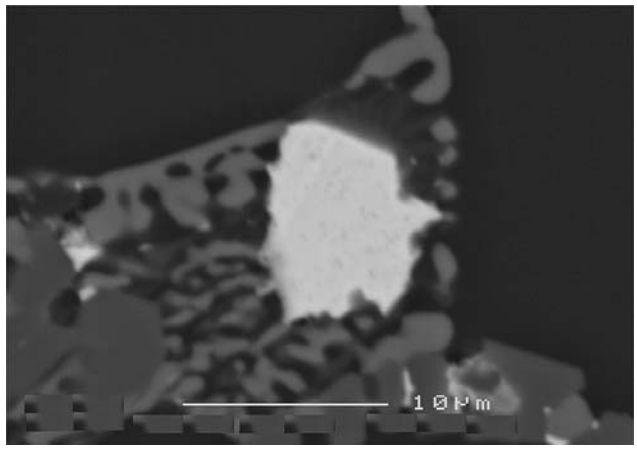

Fig. 11—High-magnification backscattered image taken from RNN alloy (RGM + 0.5 pct Sn and 0.5 pct In) showing the presence of an In_3Sn particle.

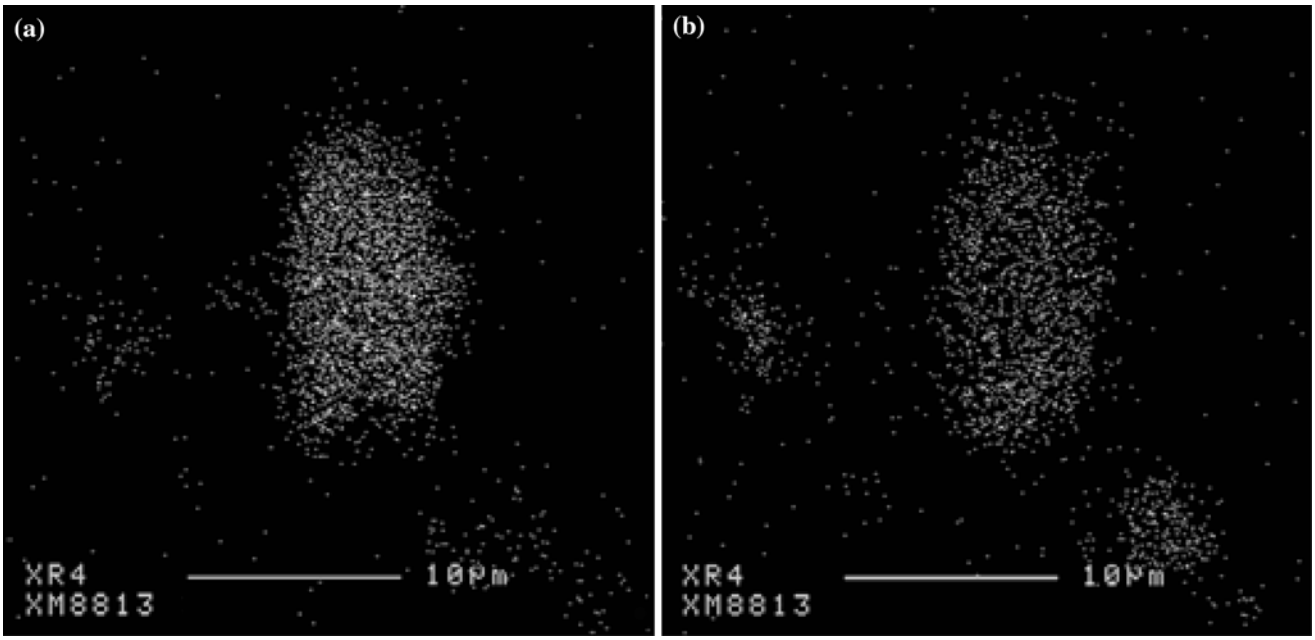

Fig. 12—X-ray images of (*a*) In and (*b*) Sn distribution in the In_3Sn particle shown in backscattered image of Fig. 11.

Table V. Chemical Composition of In_3Sn Phase Particles in As-Cast RNN Alloy Obtained from WDS Analysis

Alloy Code	Element	Wt Pct	At. Pct	Color and Shape	Phase
RNN	In	72 ± 1	72 ± 1.5	white, spherical	In_3Sn phase
	Sn	27 ± 0.5	23 ± 2		
	total	99	95		

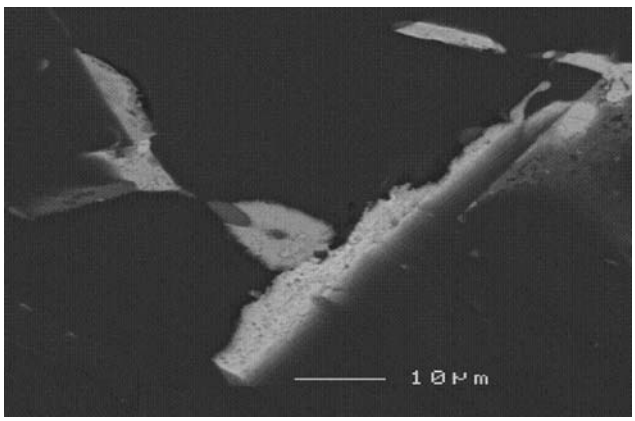

Fig. 13—Backscattered image taken from RBN alloy (RGM + 0.5 pct Bi and 1.1 pct Sn) showing the presence of Bi and Sn particles.

respectively. It is clear from these figures that there is no evidence for the formation of any intermetallic compound between Bi and Sn in the RBN alloy. The Bi-phase is not formed as an intermetallic compound with Al, because it is independently distributed. The Bi-phase is thus not uniformly distributed in the alloy structure and has a tendency to segregate and form a coarse phase. Figure 15 is a backscattered image of the R2BN alloy (RGM alloy + 0.5 pct Sn + 0.5 pct Bi), also showing the precipitation of Sn and Bi particles whose distribution is shown in Figure 16. Bismuth precipitation in the R2BN alloy was well-distributed as small particles compared to its precipitation in the RBN alloy.

B. *Mechanical Properties*

1. *As-cast condition*

Figure 17 and the tabulation in Table VI show the pertinent data relating to as-cast mechanical properties; these include the hardness, YS, UTS, and pct El of the modified grain-refined RGM alloy after the addition of Pb, Bi, and Sn, either individually or in combination. The overall results reveal that the mechanical properties ascertained for all eight experimental compositions are somewhat similar to those of the RGM alloy, in that they show better ductility at the expense of low YS and UTS. It may be observed that there is no marked difference to be seen in the YS of the as-cast samples due to the individual or combined addition of these elements.

The addition of 0.5 pct Pb causes no significant deterioration in either the hardness or the tensile properties of the RGM alloy. The same results were observed in the case of the addition of 0.5 pct Bi except for elongation, which diminishes by 35 pct compared to the RGM alloy,even though this same element has a marked influence on microstructure, as mentioned previously. On the other hand, the addition of 1.1 pct Sn reduces the hardness and UTS each by 10 pct increments compared to the RGM alloy. The lower strength and hardness values may be interpreted in terms of the presence of Sn, which results in the formation of a certain amount of soft β-Sn particles precipitated mainly at the grain boundaries. Likewise,

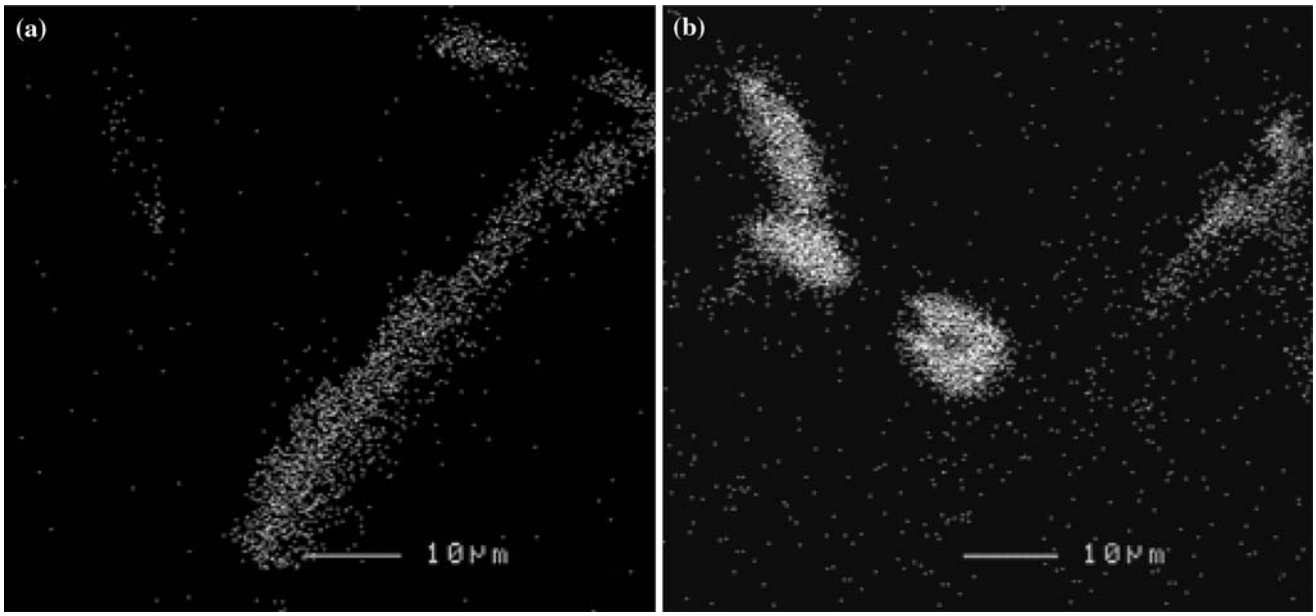

Fig. 14—X-ray images of (*a*) Bi and (*b*) Sn corresponding to the Bi and Sn particles in Fig. 13.

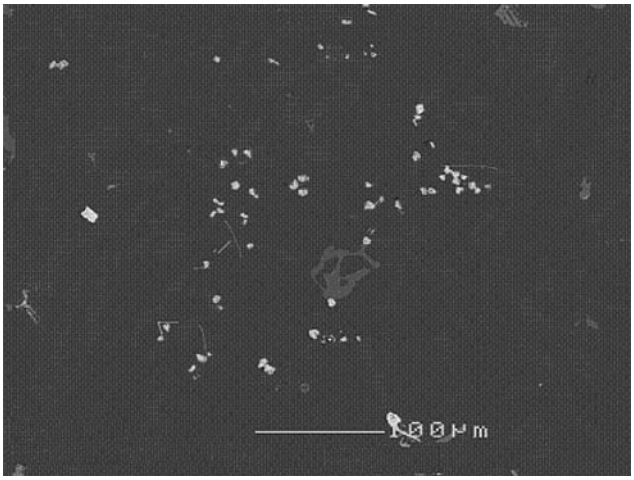

Fig. 15—Backscattered image taken from R2BN alloy (RGM + 0.5 pct Bi and 0.5 pct Sn) showing the presence of Bi and Sn particles.

and for the same reason, the elongation increases slightly by 5 pct increments.

It may also be observed that the mechanical properties of alloys containing Sn are marginally lower compared to those of alloys containing Pb. The combined addition of Pb (0.5 pct) and Bi (0.5 pct) to the RGM alloy produces better mechanical properties than does the combined addition of Bi (0.5 pct) and Sn (1.1 pct). It may also be observed that the combined addition of Sn (0.5 pct) and In (0.5 pct) to the RGM alloy leads to an improvement of 5, 10 increments, and 5 pct in YS, UTS, and pct El, respectively, compared to the addition of Sn alone.

2. *T6 and T7 heat-treated conditions*

For the modified grain-refined RGM alloy, the hardness first increases with an increase in aging temperature of up to 180 °C, decreasing thereafter as the aging temperature increases further. The changes that are to be observed in hardness values are due mainly to the size, shape, and distribution of Al_2Cu and Al_2CuMg precipitates during aging. A similar observation was reported by Reif *et al.*,[33] who produced a comparison of the precipitation behavior of Al-9 pct Si-3.5 pct Cu and Al-9 pct Si-4 pct Cu-0.5 pct Mg alloys. Their results show that the strengthening observed in the ternary Al-Si-Cu alloy after aging at 160 °C was attributed to the formation of θ'-Al_2Cu plates; also there were no Si-containing precipitates to be identified at this point. The precipitation hardening in the quaternary Al-Si-Cu-Mg alloy was ascribed to the simultaneous formation of relatively large θ' plates and small S'-Al_2CuMg needles, again without the contribution of β''-Mg/Si or other Si-containing precipitates.[34–36] Aging at 200 °C, 220 °C, and 240 °C causes a noticeable decrease in the hardness values compared to those obtained at 180 °C.

Figure 18 shows the effects of the addition of Pb, Bi, and Sn, both individually and in combination, on the hardness of T6 and T7 heat-treated alloys. In general, it can be observed that peak hardness is obtained at 180 °C for all alloys studied. A comparison of peak hardness values at 180 °C shows that the RB alloy (RGM alloy + 0.5 pct Bi) has the highest hardness compared to the other alloys. Variations occurring in hardness values with changes in aging temperature are found to follow a similar trend for all alloys investigated. The results provided in Figure 18 also show that the level of hardness in the T6-treated condition is generally lower for the RN alloy (RGM alloy + 1.1 pct Sn) than it is for other alloys. Alloy RB (RGM alloy + 0.5 pct Bi), however, displays the maximum hardness at all aging temperatures applied.

Figures 19(a) through (c) show the average YS, UTS, and pct El and their standard deviations of these alloys

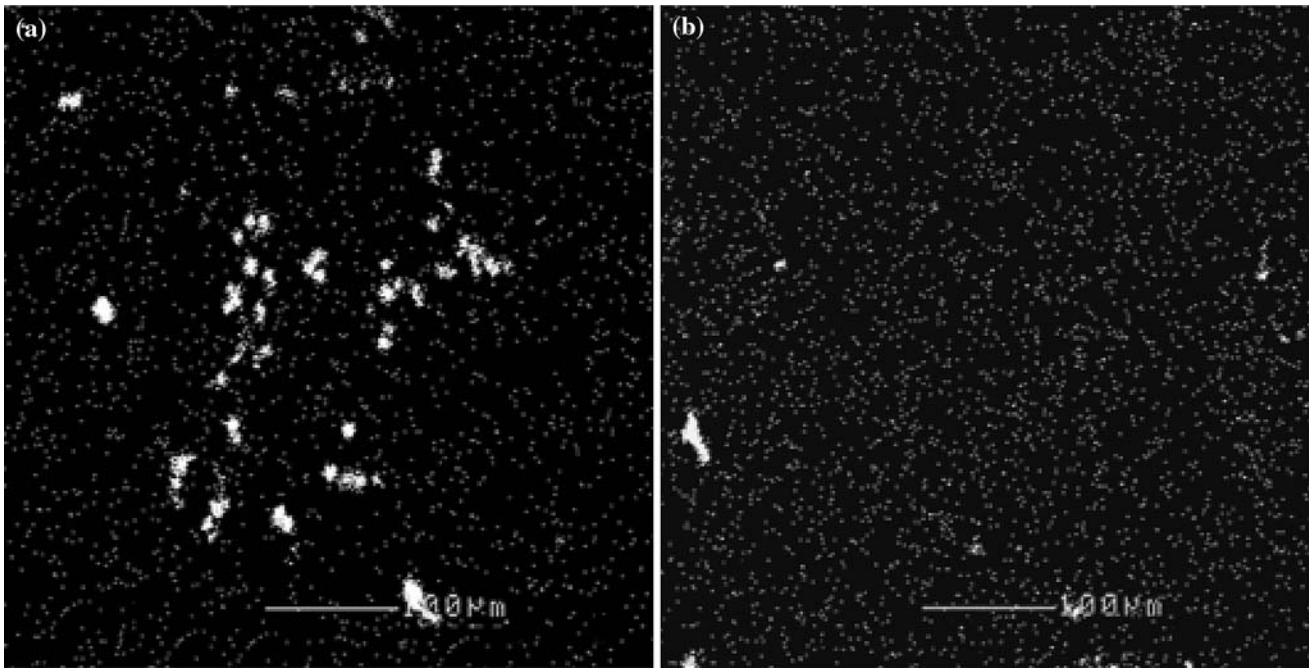

Fig. 16—X-ray images of (*a*) Bi and (*b*) Sn corresponding to the Bi and Sn particles shown in Fig. 15.

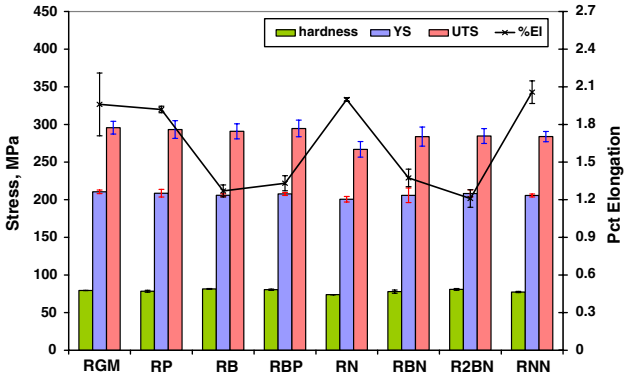

Fig. 17—Mechanical properties of experimental alloys in the as-cast condition.

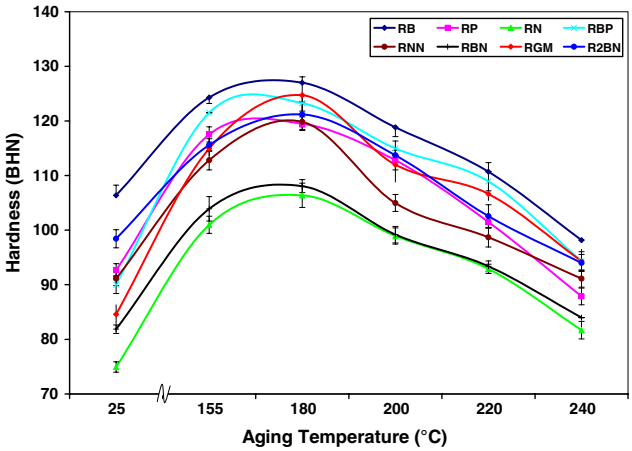

Fig. 18—Hardness of RGM alloy as a function of Pb, Bi, and Sn additions and heat treatment conditions.

Table VI. Mechanical Properties of As-Cast RGM Alloy after Addition of Pb, Bi, and Sn

Alloy Code	Yield Stress (MPa)	UTS (MPa)	Elongation (Pct)	Hardness BHN
RGM	211 ± 2	295 ± 8	1.96 ± 0.25	79.5 ± 0.1
RP	209 ± 5	293 ± 12	1.92 ± 0.03	78.5 ± 1
RB	206 ± 2	291 ± 10	1.27 ± 0.05	81.5 ± 0.5
RBP	208 ± 2	295 ± 11	1.33 ± 0.06	80.5 ± 1
RN	201 ± 4	267 ± 10	1.99 ± 0.013	74 ± 0
RBN	206 ± 10	284 ± 13	1.37 ± 0.07	78 ± 2
R2BN	208 ± 5	285 ± 10	1.21 ± 0.08	81 ± 1
RNN	206 ± 2	284 ± 7	2 ± 0.09	77.5 ± 1

plotted as a function of aging temperature. Since the value of the UTS and pct El would be influenced by any localized defect concentration, only the best results were taken into account in determining the average values plotted in Figures 19(b) and (c), in view of the fact that the scatter was too large.

In general, T6-temper produces increased strength with a corresponding loss in ductility, as well as the development of more stable mechanical properties. For example, with an aging time of 5 hours, the tensile strength increases and elongation decreases as a result of an increase in aging temperature of up to 180 °C for all alloys studied. The YS (Figure 19(a)) increases with aging temperature and attains a maximum at 180 °C for all the alloys. Softening commences when the alloy is aged at 200 °C, reaching a maximum at 240 °C. The UTS exhibits a trend similar to that shown by YS (Figure 19(b)).

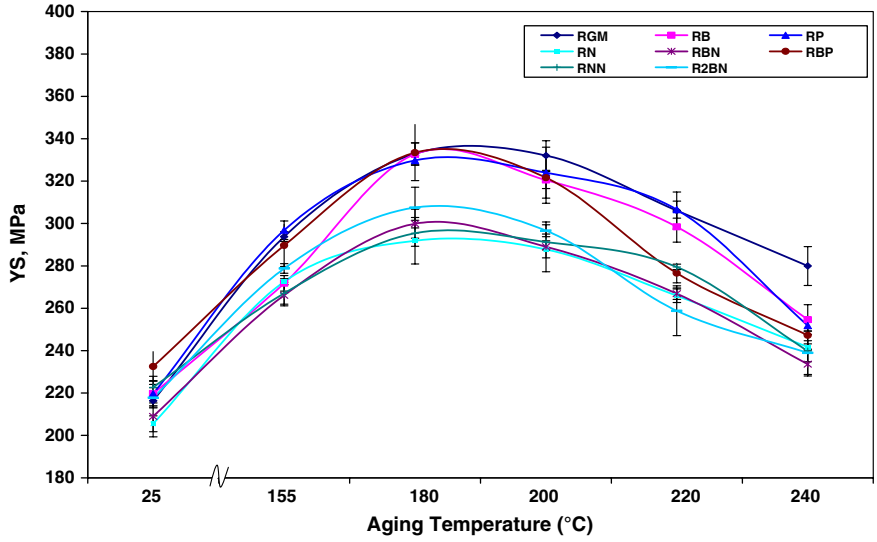

(a)

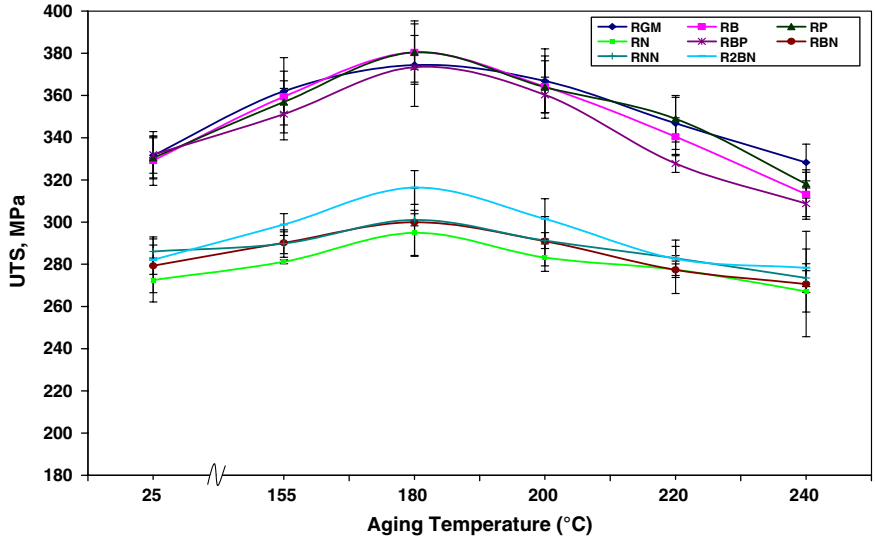

(b)

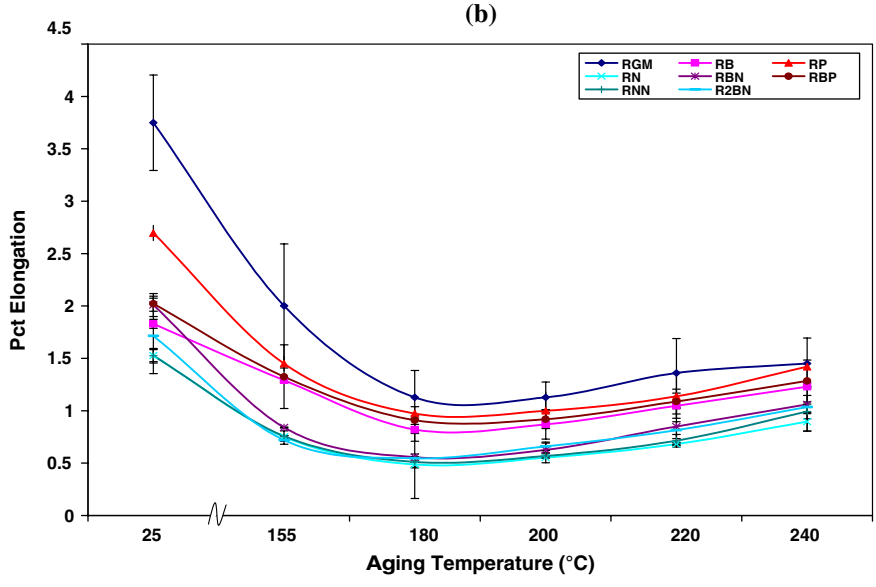

(c)

Fig. 19—Variation in (*a*) YS, (*b*) UTS, and (*c*) pct El as a function of Pb, Bi, and Sn additions and heat-treatment conditions.

It can also be observed that the RB alloy containing 0.5 pct Bi behaves in much the same way as the RP alloy containing 0.5 pct Pb at the different aging temperatures applied. On the other hand, the RN alloy shows lower tensile properties at all aging temperatures. For example, at 180 °C, the alloy YS, UTS, and pct El diminish by 10, 20, and 60 pct increments, respectively, compared to the RGM alloy. The reduced strength and ductility of the RN alloy may be attributed to the increase in percentage porosity observed in this alloy resulting from the incipient melting of β-Sn phase compared to the RGM alloy.

The addition of Bi (0.5 pct) and Pb (0.5 pct) in combination to the RGM alloy (or RPB alloy) produces properties which are more or less similar to those of the RB and RP alloys, while the RNN alloy (RGM alloy + 0.5 pct Sn + 0.5 pct In) possesses tensile properties which are higher than those obtained for the RN alloy (RGM + 1.1 pct Sn) at any of the five aging temperatures applied. For example, aging the RNN alloy for 5 hours at 180 °C is associated with increases of 1, 2, and 5 pct in YS, UTS, and pct El, respectively, compared to the values exhibited by the RN alloy. It is evident from the results that the Sn-In interaction enhances the alloy strength parameters above those obtained from the RN alloy, which contains only the addition of Sn. Similarly, a combined addition of Sn and Bi improves the tensile properties significantly compared to the RN alloy.

IV. CONCLUSIONS

The following conclusions may be drawn from the experiments conducted to study the influence of additions of Pb, Bi, and Sn on the microstructure and mechanical properties of modified grain-refined Al-10.8 pct Si near-eutectic alloy.

1. The addition of lead individually has no significant effect on the microstructure and mechanical properties of the modified grain-refined Al-10.8 pct Si alloy in as-cast and heat-treated conditions.
2. The addition of 0.5 pct bismuth to the modified grain-refined Al-10.8 pct Si alloy counteracts the modifying effect of Sr, leading to a noticeable coarsening of the eutectic Si particles.
3. Tin precipitates as particles of β-Sn within the Al_2Cu network when added individually to the modified grain-refined Al-10.8 pct Si alloy. When added in combination with indium, it precipitates mainly in the form of irregular In_3Sn phase particles. Tin, when added individually, causes a decrease in the UTS and hardness of the alloy in the as-cast and artificially-aged conditions. However, the addition of Sn causes an increase in elongation only in the as-cast condition.
4. No marked difference in the YS of the as-cast samples is to be observed as a result of adding Pb, Bi, and Sn, whether individually or in combination.
5. In the case of the modified grain-refined Al-10.8 pct Si alloy with the addition of Pb, Bi, and Sn, whether individually or in combination, peak hardness is observed at the 180 °C/5 hours aging condition.
6. The combined addition of Pb and Bi to the modified grain-refined Al-10.8 pct Si alloy provides better mechanical properties in the as-cast and aged conditions than is provided by a combined addition of Bi and Sn.
7. The mechanical properties regarding the T6-condition display similar trends for all the alloys studied.

ACKNOWLEDGMENTS

The authors express grateful acknowledgement for financial and in-kind support received from the National Sciences and Engineering Research Council of Canada, GM Powertrain Group, and Corporativo Nemak. Thanks are also due to Mr. Lang Shi at the Microanalysis Laboratory, Earth and Planetary Sciences, McGill University, for carrying out the EPMA analyses.

REFERENCES

1. C.M. Sonsino and J. Ziese: *Int. J. Fatigue*, 1993, vol. 15 (2), pp. 75–84.
2. H. Liao and G. Sun: *Scripta Mater.*, 2003, vol. 48, pp. 1035–39.
3. A.M.A Mohamed, F.H. Samuel, A.M. Samuel, H.W. Doty, and S. Valtierra: *Proc. Int. Symp. on Aluminum: from Raw Materials to Applications*, Conf. Metallurgists (CIM), Montreal, Oct. 1–4, 2006, G. Dufour, F. Paray, and J. Tessier, eds., Montreal, Quebec, Canada, 2006, pp. 167–83.
4. A.M.A Mohamed, F.H. Samuel, A.M. Samuel, H.W. Doty, and S. Valtierra: *Proc. 18th Canadian Materials Science Conf. (CMSC)*, Montreal, June 2006, Session 10, Aluminum II, paper no. 10.3.
5. H. Liao, Y. Sun, and G. Sun: *J. Mater. Sci.*, 2002, vol. 37, pp. 3489–95.
6. G.K. Sigworth: *AFS Trans.*, 1983, vol. 91, pp. 7–16.
7. M.M. Haque: *J. Mater. Process. Technol.*, 1995, vol. 55, pp. 193–98.
8. H. Liao, Y. Sun, and G. Sun: *Mater. Sci. Eng. A*, 2003, vol. 358, pp. 164–70.
9. H. Liao and G. Sun: *Mater. Sci. Technol.*, 2004, vol. 20, pp. 521–27.
10. K. Venkateswarlu, M. Chakraborty, and B. Murty: *Mater. Sci. Eng. A*, 2004, vol. 364, pp. 75–83.
11. L. Pio, S. Sulaiman, A. Hamouda, and M. Ahmad: *J. Mater. Process. Technol.*, 2005, vols. 162–163, pp. 435–41.
12. J. Grobner, D. Mirkovi, and R. Fetzer: *Mater. Sci. Eng. A*, 2005, vol. 395, pp. 10–21.
13. A. Smolej, V. Dragojevič, and T. Smolar: U.S. Patent 6248188B1, 2001.
14. W. König and D. Erinski: *Manuf. Technol.*, 1983, vol. 32 (2), pp. 535–40.
15. Y. Yang: U.S. Patent 6,511,633, 2003.
16. S. Sircar: *Mater. Sci. Forum*, 1996, vols. 217–222, pp. 1975–1800.
17. S. Subhasich: U.S. Patent 5,587,029, 1996.
18. O. Melikhova, J. Čížek, J. Kuriplach, J. Faltus, and I. Stulikova: *Mater. Struct.*, 2001, vol. 8 (2), pp. 61–67.
19. J. Faltus and K. Plaček: *Proc. 6th Int. Metall. Symp. METAL 97*, T. Prnka, ed., Czech Republic, 1997, vol. 3, p. 131.
20. H. Torabin, J.P. Pathak, and S.N. Tiwari: *Wear*, 1994, vol. 177 (1), pp. 47–54.
21. S. Murali, K.T. Kashyap, K.S. Ramen, and K.S.S. Murthy: *Scripta Metall. Mater.*, 1993, vol. 29, pp. 1421–26.

22. V.S. Grebenkin, T.V. Sil'chenko, A.A. Gorshkov, and Y. Dzykovich: *Met. Sci. Heat Treat.*, 1972, vol. 3, pp. 50–54.
23. A.M.A Mohamed, F.H. Samuel, A.M. Samuel, H.W. Doty, and S. Valtierra: *Metall. Mater. Trans. A*, 2008, vol. 39A, pp. 490–501.
24. N.P. Pillai and T.R. Anantharaman: *Trans. TMS-AIME*, 1968, vol. 24 (2), pp. 2025–27.
25. J.I. Cho and C.R. Loper: *AFS Trans.*, 2000, vol. 104, pp. 359–67.
26. A.V. Kurdyumov and S.V. Inkin: *Liteinoe Proizvodstvo*, 1986, vol. 6, pp. 28–29.
27. F.H. Samuel, A.M. Samuel, and H.W. Doty: *AFS Trans.*, 1996, vol. 104, pp. 893–901.
28. H. Rosenbaum and D. Turnbull: *Acta Metall.*, 1959, vol. 7, pp. 664–74.
29. J.V. Suchtelen: *J. Cryst. Growth*, 1978, vol. 43, pp. 28–46.
30. C.W. Meyers: *AFS Trans.*, 1985, vol. 93, pp. 741–50.
31. C.J. Machovec, G.E. Byczynski, J.W. Zindel, and L.A. Godlewski: *AFS Trans.*, 2000, vol. 108 (76), pp. 439–44.
32. *ASM Metals Handbook*, vol. 3, *Alloy Phase Diagrams*, ASM INTERNATIONAL, Materials Park, OH, 1992.
33. W. Reif, J. Dutkiewicz, R. Ciach, S. Yu, and J. Król: *Mater. Sci. Eng. A*, 1997, vols. 224–236, pp. 165–68.
34. M. Moustafa, F.H. Samuel, H.W. Doty, and S. Valtierra: *Int. J. Cast Met. Res.*, 2002, vol. 14, pp. 235–53.
35. P. Ouellet and F.H. Samuel: *J. Mater. Sci.*, 1999, vol. 34, pp. 4671–97.
36. G. Wang, X. Bain, W. Wang, and J. Zhang: *Mater. Lett.*, 2003, vol. 57, pp. 4083–87.